Human Telomerase RNA Pseudoknot and Hairpin Thermal Stability with Glycine Betaine and Urea: Preferential Interactions with RNA Secondary and Tertiary Structures†

Jeffrey J. Schwinefus,* Mikhail J. Kuprian,‡ John W. Lamppa,‡ Wolf E. Merker,‡ Kristin N. Dorn, and Gregory W. Muth

Department of Chemistry, St. Olaf College, Northfield, Minnesota 55057

Received December 22, 2006; Revised Manuscript Received April 20, 2007

ABSTRACT: Thermal denaturation of the human telomerase RNA (hTR) ΔU177 pseudoknot and hTR p2b hairpin was investigated by dual UV-wavelength absorbance spectroscopy in aqueous glycine betaine and urea solutions. The hTR ΔU177 pseudoknot contains two helix−loop interactions that comprise the tertiary structure, as well as a GC-rich 6 bp stem (stem 1) and an AU-rich 9 bp stem (stem 2). The p2b hairpin also contains GC-rich stem 1 and a unique uridine-rich helix with a pentaloop. Glycine betaine stabilizes the pseudoknot tertiary structure in 135 m*m* NaCl and facilitates only a minor destabilization of tertiary structure in 40 m*m* NaCl. As with double-helical DNA, glycine betaine interacts more strongly with the surface area exposed upon unfolding of GC-rich stem 1 than either AU-rich stem 2 or the hairpin uridine-rich helix. Urea was shown to destabilize all RNA pseudoknot and hairpin secondary and tertiary structures but exhibits a stronger preferential interaction with AU-rich stem 2. Correlating these interactions with water-accessible surface area calculations indicates that the extent of interaction of glycine betaine with the surface area exposed upon RNA unfolding decreases as the nonpolar character of the unfolded RNA surface increases. As expected, the extent of interaction of urea with the surface area exposed for unfolding RNA increases as the fraction of amide functional groups increases. However, interaction of urea with amide functional groups alone cannot explain the stronger preferential interaction of urea with AU-rich stem 2. Interaction of urea with adenine relative to guanine and cytosine bases or sequence-dependent hydration is proposed for the stronger preferential interaction of urea with AU-rich duplexes.

The thermodynamics of protein and RNA folding and double-stranded (ds) DNA helix formation are strongly perturbed by small, neutral organic cosolutes such as polyhydric alcohols and sugars, amino acids, N-methylated glycines, and urea. The stability of these folded biopolymer structures can be either enhanced or attenuated depending on the preferential interaction of cosolutes for the solvent-accessible surface area (ASA)[1] exposed in the unfolding process. Since cosolutes form a substantive portion of the cellular milieu, understanding how the preferential interaction of cosolutes correlates with changes in the surface area of biopolymers in contact with solvent is fundamentally important in understanding biopolymer folding.

To date, the influence of the cosolutes glycine betaine and urea on the protein and dsDNA helix unfolding transition has been studied extensively. Glycine betaine is a protein stabilizer, increasing protein thermal transition temperatures (T_m) by 5−10 °C at 3−4 M glycine betaine (*1*). Urea is a strong protein denaturant (*2*, *3*). Cells that accumulate urea to any appreciable extent often accumulate other cosolutes, such as glycine betaine or trimethylamine *N*-oxide (TMAO), to offset urea's protein destabilizing effects (*4*, *5*). However, glycine betaine and urea are both dsDNA destabilizers; dsDNA thermal transition temperatures decrease linearly with both increasing glycine betaine (*6*, *7*) and urea (*8*−*10*) concentrations. Glycine betaine is noted for its "isostabilizing" ability, eliminating the dependence of T_m on GC composition with almost no effect on the poly(dAdT) thermal transition (*6*, *7*). Urea lacks glycine betaine's isostabilizing ability, preferring to destabilize AT base pairs to a greater extent than GC base pairs (*9*, *11*).

Despite the efforts to elucidate a unifying protein and dsDNA thermal unfolding mechanism with cosolutes, the influence of glycine betaine and urea on RNA thermal unfolding has received scant attention. This is rather surprising since RNA secondary and tertiary unfolding in urea solutions mimics elements of urea-induced protein and dsDNA destabilization (*12*). As with dsDNA, urea destabilizes RNA tertiary and secondary structure but has little effect on other fundamental characteristics of the unfolding transition (*12*−*16*). Interestingly, urea did not demonstrate a preference for short AU-rich RNA duplexes over short GC-rich duplexes in the study of Shelton et al. (*15*), although

† This research was supported by an award from Research Corp. (CC6299) and an award from the Merck Institute for Science Education. This research was also supported in part by a grant to St. Olaf College from the Howard Hughes Medical Institute through the Undergraduate Science Education Program.

* To whom correspondence should be addressed. Phone: (507) 646-3105. Fax: (507) 646-3968. E-mail: schwinef@stolaf.edu.

‡ These authors contributed equally to this work.

[1] Abbreviations: ASA, water-accessible surface area; ΔASA, change in water-accessible surface area.

10.1021/bi602637v CCC: $37.00
Published on Web 07/14/2007

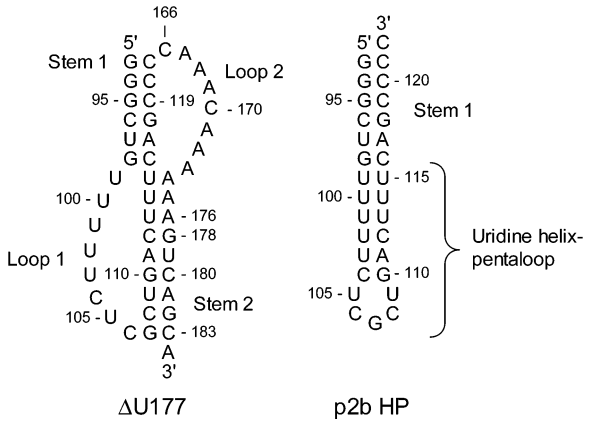

FIGURE 1: Sequence and secondary structure of the ΔU177 hTR pseudoknot and the p2b hTR hairpin (HP). Stem 1 is identical in the two structures, except for the 3′ C overhang in the p2b hTR hairpin.

this preference may have been attenuated sufficiently to preclude its observation at the high ionic strength (0.5−1.0 M NaCl) that was used (*11*). However, TMAO can counteract urea destabilization of RNA tertiary structure just as it can with folded proteins (*12*). It is significant, and rather surprising, that chemically dissimilar proteins and RNA behave similarly in urea and TMAO solutions. A complete understanding of the sensitivity of protein, RNA, and dsDNA structures to solvent composition is necessary for the identification of common themes in the biopolymer folding process. In addition, these cosolutes could be used to thermodynamically distinguish between RNA secondary and tertiary structures as well as GC-rich versus AT-rich (or possibly AU-rich) nucleic acid duplexes.

In this study, we quantify the enhanced accumulation of glycine betaine and urea at the newly exposed ASA of the human telomerase RNA (hTR) ΔU177 pseudoknot and the hTR p2b hairpin (HP) (Figure 1) during thermal denaturation. The hTR ΔU177 pseudoknot is a RNA construct including all of p3 (stem 2) and j2b/3 (loop 1) and the conserved regions of p2b (stem 1) and j2a/3 (loop 2) of the 451-nucleotide telomerase RNA with the single-nucleotide U177 bulge in stem 2 removed (*17*). Removal of the single-nucleotide bulge in stem 2 eliminates the alternative p2b hairpin conformation in equilibrium with the wild-type (wt) pseudoknot while maintaining the same base pairing and tertiary interactions that have been observed for the wt pseudoknot (*17*, *18*). Essential for proper function of human telomerase, the hTR ΔU177 pseudoknot tertiary structure is formed from uridine-rich loop 1 lying in the major groove of stem 2 and adenine-rich loop 2 lying in the minor groove of stem 1. As mentioned, the hTR p2b hairpin is an equilibrium form of the wt hTR pseudoknot containing stem 1 as well as a unique uridine-rich double helix and pentaloop formed via loop 1 and stem 2 bases (*18*). The ΔU177 pseudoknot and p2b hairpin structures were chosen for this study because the unfolding thermodynamics of these RNA structures in cosolute-free solutions are well documented and only monovalent ions are required to maintain RNA tertiary structure. Also, NMR solution structures of both RNAs exist, permitting analysis of water-accessible surface areas. Additionally, the secondary and tertiary structures of the two RNAs are chemically dissimilar except for stem 1, which can be used as a metric of consistency for the unfolding studies between the two RNAs.

To quantify the enhanced accumulation of glycine betaine and urea at the newly exposed ASA of these RNA structures, we have determined the change in preferential interaction coefficients $\Delta\Gamma_{\mu_3,m_4}$ [at a constant chemical potential of cosolute (μ_3) and a constant molality of salt (m_4)] using the dependence of the thermal transition temperatures on water activity. We seek to find unifying themes for biopolymer unfolding in aqueous glycine betaine and urea solutions by correlating $\Delta\Gamma_{\mu_3,m_4}$ for the secondary and tertiary structures in the hTR ΔU177 pseudoknot and the hTR p2b hairpin with the change in accessible surface area (ΔASA) and the chemical functional groups exposed upon unfolding. If RNA and protein tertiary structures exhibit similar behavior in aqueous cosolute solutions, as seen with TMAO and urea, we hypothesize glycine betaine should have little or even a stabilizing influence on the ΔU177 pseudoknot tertiary structure. In addition, using low to moderate concentrations of salt (40 and 135 m*m* NaCl), we predict glycine betaine to interact preferentially with GC-rich RNA duplexes and urea to interact preferentially with AU-rich RNA duplexes, comparable to that seen with GC-rich and AT-rich dsDNA.

MATERIALS AND METHODS

RNA Synthesis and Purification. The hTR ΔU177 pseudoknot was prepared by *in vitro* transcription using His_6-tagged T7 RNA polymerase as described by Milligan et al. (*19*). Reaction conditions were 40 mM Tris-HCl (pH 7.6), 50 mM NaCl, 20 mM $MgCl_2$, 2 mM spermidine, 0.05% Triton X-100, 6 mM dithiothreitol, 5 mM nucleotide triphosphates, 1 unit/mL thermostable inorganic pyrophosphatase (New England Biolabs), 0.3 mg/mL T7 RNA polymerase, and 15 μg/mL dsDNA. The dsDNA template (IDT DNA, Coralville, IA) was designed with the hTR ΔU177 pseudoknot sequence (*17*) downstream of a T7 promotor and used without further purification. Transcription reaction mixtures were ethanol precipitated and purified by PAGE, electro-eluted, and exhaustively dialyzed against 10 mM sodium phosphate buffer (pH 7.0) (16 m*m* Na^+) with either 40 or 135 m*m* NaCl. The hairpin RNA sequence r(GGG CUG UUU UUC UCG CUG ACU UUC AGC CCC) was purchased from IDT DNA, exhaustively dialyzed against 10 mM sodium phosphate buffer (pH 7.0) with either 40 or 135 m*m* NaCl, and used without further purification.

Solutes. Reagent-grade glycine betaine (*N*,*N*,*N*-trimethylglycine) and urea were purchased from Sigma and used without further purification. Solutions for thermal melting studies were prepared using a 10 mM sodium phosphate buffer (pH 7.0) with either 40 or 135 m*m* NaCl. Phosphate buffer components $NaH_2PO_4 \cdot H_2O$, Na_2HPO_4, and NaCl were all purchased from Fisher Scientific. All buffers were prepared gravimetrically to establish both the molarity and molality of buffer components.

RNA Thermal Denaturation. RNA/cosolute solutions were prepared gravimetrically by mixing the stock RNA solution, cosolute, and sodium phosphate buffer to ensure constant RNA and NaCl molality with varying cosolute molality. Cosolute solutions were prepared in 0.5 *m* increments with a maximum concentration of 2 *m*. RNA concentrations were 1−3 μM. Final NaCl concentrations were either 40 or 135

m*m*. After the addition of glycine betaine or urea, the pH of the solutions was within 0.4 pH unit of pH 7.0. Solutions were degassed with either vacuum or nitrogen prior to thermal denaturation. RNA thermal transitions were monitored at 260 and 280 nm simultaneously using a Cary 100 UV−visible spectrophotometer (Varian) equipped with a Peltier temperature controller. Teflon-stoppered quartz cuvettes from Fisher Scientific with a path length of 1 cm were used. RNA samples were heated at a rate of 0.3 °C/min from 20 to 100 °C, and absorbance readings were collected every 0.2 °C.

Analysis of UV-Absorbance Data. First derivatives of the absorbance versus temperature data (d*A*/d*T*) were obtained using sliding linear fits of 1−2 °C on the absorbance data, the slopes of the linear fits being the smoothed derivatives of the absorbance data sets. The smoothed derivatives were subjected to linear baseline interpolation (see the Supporting Information). The smoothed derivatives were subjected to nonlinear least-squares parameter analysis of $T_{m,i}$, $\Delta H^{o}_{T_{m,i}}$ (van't Hoff enthalpy for RNA unfolding at T_m), A_i^{260} (total UV absorption change at 260 nm), and A_i^{280} (total UV absorption change at 280 nm) for all *i* transitions, assuming a sequential two-state unfolding model (*20*). Two nonlinear least-squares fitting algorithms were used. The first method used the Levenberg−Marquardt algorithm with Origin (OriginLab) where the 260 and 280 nm data were fit independently and the parameters averaged for the two wavelengths. The second method used the T-Melt algorithm (J. Christopher, Texas A&M University, College Station, TX) where the 260 and 280 nm data were fit simultaneously using the same thermodynamic parameters (*21*). Both methods gave nearly identical results. The results presented in this work were obtained solely from the T-Melt program.

Preferential Interaction Coefficients. The driving force for the T_m increase or decrease of a biopolymer unfolding transition in glycine betaine or urea solutions is the unfavorable or favorable interaction of these cosolutes with the newly exposed biopolymer ASA during the unfolding process. Since these cosolutes do not necessarily bind at localized sites as ligands, accumulation or exclusion at the biopolymer surface is best characterized by preferential interaction coefficients. Preferential interaction coefficients (Γ_{μ_3,m_4}) are generally defined in the context of a dialysis experiment. In aqueous four-component solutions with a vanishingly small concentration of biopolymer (component 2), a fixed concentration of salt (component 4), and a variable concentration of uncharged cosolute (component 3), the preferential interaction coefficient is given by (here component 1 is water) (*22*)

$$\Gamma_{\mu_3,m_4} = (\partial m_3/\partial m_2)_{T,P,\mu_3,m_4} \quad (1)$$

where m_i is the molality of species *i* and μ_3 is the chemical potential of the cosolute. Any preferential accumulation (exclusion) of cosolute at the biopolymer surface would lead to a larger (smaller) concentration of cosolute in some local domain around the biopolymer relative to bulk and $\Gamma_{\mu_3,m_4} > 0$ (<0) (*22*−*26*).

In general, the concentration-dependent effect of cosolutes on the observed equilibrium constant K_{obs} for a biopolymer structural transition is related to $\Delta\Gamma_{\mu_3,m_4}$, the difference in Γ_{μ_3,m_4} between the unfolded biopolymer and folded biopolymer weighted by the stoichiometric coefficients in the biopolymer reaction equation, by

$$(\partial \ln K_{obs}/\partial \ln a_3)_{T,P,m_2,m_4} = \Delta\Gamma_{\mu_3,m_4} \quad (2)$$

where a_3 is the activity of cosolute (*22*, *26*−*28*). Values of $\Delta\Gamma_{\mu_3,m_4}$ represent the preferential interaction of cosolute with the solvent-accessible biopolymer surface area exposed during the unfolding transition (*24*). Positive values (negative values) of $\Delta\Gamma_{\mu_3,m_4}$ indicate accumulation (exclusion) of cosolute at the newly exposed ASA of an unfolded biopolymer, because cosolute interaction is more thermodynamically favorable (unfavorable) with the unfolded structure than the folded structure. Values of $\Delta\Gamma_{\mu_3,m_4}$ are often identified with the change in the amount of cosolute associated with the unfolded and folded structures in the unfolding transition (*27*, *28*).

Using eq 2, the dependence of the melting temperature T_m on a_3 can be related to $\Delta\Gamma_{\mu_3,m_4}$ by

$$dT_m^{-1}/d(\ln a_3) = R/\Delta H^{\circ}_{T_m} \times \Delta\Gamma_{\mu_3,m_4} \quad (3)$$

where *R* is the ideal gas constant (*26*). With the Gibbs−Duhem relation (*29*), eq 3 can be rewritten as

$$dT_m^{-1}/d(\ln a_1) = -R \times m_1/\Delta H^{\circ}_{T_m} \times \Delta\Gamma_{\mu_3,m_4}/m_3 \quad (4)$$

where a_1 is the activity of water and m_1 (55.56 mol/kg) is the molality of water. For our purposes, inverse melting temperatures (T_m^{-1}) of the hTR ΔU177 pseudoknot and p2b hairpin were plotted versus ln a_1 and eq 4 was used to extract $\Delta\Gamma_{\mu_3,m_4}/m_3$ for the RNA secondary and tertiary structures. Additionally, the number of waters released in the RNA unfolding transition, Δn_1, can be related to $\Delta\Gamma_{\mu_3,m_4}/m_3$ by (*30*)

$$\Delta n_1 = m_1 \times \Delta\Gamma_{\mu_3,m_4}/m_3 \quad (5)$$

Equation 5 indicates that changes in the cosolute distribution around RNA with the unfolding transition must be balanced by changes in the water distribution.

Water activities were determined from osmotic coefficients ϕ (*31*) for aqueous urea (*32*) and glycine betaine (*33*) solutions using the expression osmolality $\equiv \phi m_3 = -m_1 \ln a_1$ ($m_1 = 55.56$ mol/kg). To account for the addition of NaCl, water activities were determined from the sum of NaCl and cosolute osmolalities. The osmolality of NaCl and the osmolality of either urea or glycine betaine are additive up to at least 2 *m* cosolute (*11*). Sodium chloride osmolalities were determined using a Wescor vapor pressure osmometer (model 5520). Water activities were not corrected for the 10 mM sodium phosphate buffer. We made no temperature correction for water activity in our data analysis.

ASA Calculations. Water-accessible surface area (ASA) calculations of the folded hTR ΔU177 pseudoknot and p2b hairpin used Protein Data Bank (PDB) entries 1YMO and 1NA2, respectively. Water-accessible surface areas of the 20 conformers in PDB entry 1YMO and the 18 conformers in PDB entry 1NA2 were calculated using Surface Racer (*34*) with a probe radius of 1.4 Å and the set of van der Waals radii from Richards (*35*).

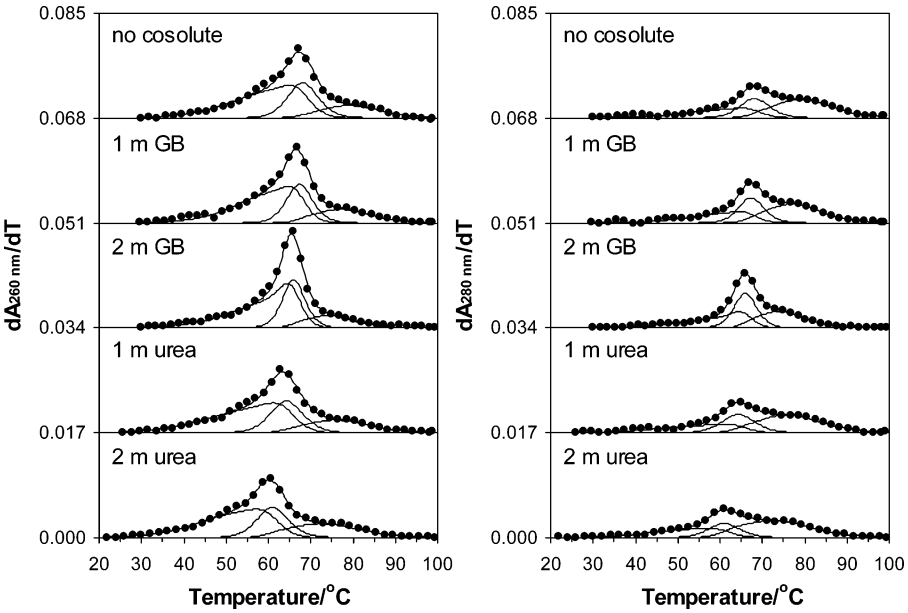

FIGURE 2: Absorbance first-derivative melting profiles at 260 and 280 nm for 2.25 μM ΔU177 hTR pseudoknot in 135 m*m* NaCl solutions containing either glycine betaine (GB) or urea. Composite fits (solid lines) are superimposed on the experimental data (every fifth data point shown). The three individual transitions of the composite fit are shown as solid lines. Curves are offset on the *y*-axes to illustrate trends in peak position with added cosolute.

To compute the ASA for each conformer of the unfolded ΔU177 pseudoknot with nucleotides in their stacked conformation, PyMol (DeLano Scientific LLC, Palo Alto, CA) was used to rotate the C166 O3*−A167 P bond 90° counterclockwise and rotate the C106 O3*−G107 P bond 120° clockwise. These bonds were chosen because rotation about these bonds efficiently breaks hydrogen bonding between other coplanar bases in the folded pseudoknot. For some conformers, rotation about these bonds led to atom overlap. In these cases, additional rotation about the C166 O3*−A167 P bond was performed or rotation about either the C166 O5*−C166 P bond or the G107 O5*−G107 P bond was substituted for, or coupled with, the original rotations. For the p2b hairpin, the G107 O3*−C108 P bond was rotated counterclockwise 90°. The ASA of each unfolded conformer with nucleotides in an unstacked conformation was determined after rotation about either the O3*−P or O5*−P bond between bases to eliminate adjacent base−base interactions.

The change in accessible surface area (ΔASA) was defined as the difference in average conformer ASA for the unfolded and folded RNA structures. To determine the ΔASA for stem 1 and stem 2 in the ΔU177 pseudoknot, loop 1 bases 100−105 and loop 2 bases 167−173 were excised before the ASA of the folded stems was calculated. Initial and terminal bases from the loops were left intact on the folded stems, since these loop anchor points are expected to be in or near their current positions even when loops 1 and 2 are denatured from the folded structure. To determine the ΔASA for unfolded RNA with nucleotides in a half-stacked conformation, the ASAs for the unstacked and stacked nucleotide conformations were averaged.

To establish correlations between distinct chemical functional groups exposed in ΔASA and $\Delta\Gamma_{\mu_3,m_4}$, we used the definition of anionic oxygen, amide, other polar, and nonpolar ASA from Hong et al. (*22*). Briefly, the anionic oxygen ASA was defined as the ASA of the two oxygens covalently bonded to each phosphate. The amide ASA was defined as the ASA of nitrogens and carbonyl oxygens of amide functional groups found on N1, O2, N3, and O4 of uridine; N1, N3, and O2 of cytosine; and N1 and O6 of guanine; adenine has no amide ASA. The other polar ASA was the amount of oxygen and nitrogen ASA other than that derived from anionic oxygen or amide ASA. The nonpolar ASA was the ASA of carbons.

RESULTS

ΔU177 hTR Pseudoknot Unfolding. The ΔU177 hTR pseudoknot unfolds in three sequential transitions corresponding to the loop 1 and loop 2 tertiary interaction, AU-rich stem 2, and finally GC-rich stem 1 (*17*). Figure 2 shows representative ΔU177 pseudoknot 260 and 280 nm first-derivative UV-absorbance melting curves in glycine betaine and urea solutions at 135 m*m* NaCl. Table 1 lists the melting temperatures and enthalpy changes determined from the sequential unfolding model for the ΔU177 pseudoknot secondary and tertiary structures in cosolute-free solutions at 40 and 135 m*m* NaCl. A table listing melting temperatures and enthalpy changes for the ΔU177 pseudoknot secondary and tertiary structures at all cosolute molalities can be found in the Supporting Information.

We found the transitions of the ΔU177 pseudoknot to be reversible, although the RNA was subject to a high degree of degradation, potentially due to hydrolysis at high temperatures. Polyacrylamide gel electrophoresis of the heated and cooled UV-spectrophotometric samples identified the folded ΔU177 pseudoknot with numerous degradation products. Therefore, all RNA samples were thermally denatured once and then discarded.

Thermodynamic parameters collected at 1 M NaCl were used to predict enthalpy changes of 85 and 59 kcal/mol for the melting of stem 2 with the 3′ A overhang and stem 1, respectively (*36*, *37*). Our measured enthalpy changes in Table 1 are in good agreement with these values, approximately 1 and 11% less than that predicted for

Table 1: Thermodynamic Parameters for Unfolding the ΔU177 hTR Pseudoknot and p2b hTR Hairpin Secondary and Tertiary Structures in Cosolute-Free Solutions[a]

	40 m*m* NaCl		135 m*m* NaCl	
	T_m (°C)	$\Delta H^\circ_{T_m}$ (kcal/mol)	T_m (°C)	$\Delta H^\circ_{T_m}$ (kcal/mol)
ΔU177 pseudoknot tertiary structure	52.6 ± 0.7	34.8 ± 0.9	60.5 ± 0.8	34.2 ± 1.0
ΔU177 pseudoknot stem 2	59.3 ± 0.1	84.0 ± 0.7	67.7 ± 0.1	86.3 ± 0.8
ΔU177 pseudoknot stem 1	71.0 ± 0.1	52.5 ± 0.7	79.9 ± 0.1	52.7 ± 1.2
p2b hairpin uridine helix and pentaloop	47.4 ± 0.1	36.0 ± 0.2	50.6 ± 0.1	33.3 ± 0.2
P2b hairpin stem 1	64.5 ± 0.1	48.4 ± 0.3	71.3 ± 0.1	53.1 ± 0.3

[a] All RNA solutions were prepared in a 10 mM sodium phosphate buffer (pH 7.0). Values are averages of a minimum of two independent experiments with standard errors from the sequential transition fitting algorithm. Thermodynamic parameters for unfolding of the ΔU177 hTR pseudoknot and p2b hTR hairpin in glycine betaine and urea solutions can be found in the Supporting Information.

stem 2 and stem 1, respectively. We find the total enthalpy change of the three transitions in 135 m*m* NaCl (173 kcal/mol) is consistent with the total enthalpy change of unfolding the wt hTR pseudoknot in 200 mM NaCl (164.7 kcal/mol) (*18*).

The asymmetry in the ΔU177 tertiary unfold is a consequence of the proximity in temperature of the stem 2 unfold. In the sequential transition model, the absorbance change for a given transition (and, hence, the derivative with respect to temperature) is dependent on the other transitions in which that transition appears (*20*). Thus, the melting temperatures (T_m) do not necessarily occur at the transition maxima in Figure 2. However, as seen almost exclusively in Figure 2, as the cosolute molality increases, the temperatures corresponding to the transition maxima decrease with a concomitant decrease in the T_ms. However, unlike urea, glycine betaine seems to have little effect on the T_m of the tertiary unfolding transition. Additionally, the tertiary, stem 2, and stem 1 transitions narrow and increase in amplitude with increasing glycine betaine molality because of glycine betaine's isostabilizing capability (*6*, *7*). The narrower transitions result in a significantly higher van't Hoff enthalpy; $\Delta H^\circ_{T_m}$ increases on average by approximately 15% for the tertiary unfold, 30% for the stem 2 unfold, and 15% for the stem 1 unfold at 2 *m* glycine betaine relative to 0 *m* glycine betaine (see the Supporting Information). Unlike glycine betaine, urea lowers $\Delta H^\circ_{T_m}$ for the three transitions in 40 and 135 m*m* NaCl by 10−20% at 2 *m* relative to 0 *m* urea (see the Supporting Information). This attenuation in $\Delta H^\circ_{T_m}$ is consistent with melting an mRNA pseudoknot (*13*) and dsDNA (*10*) in aqueous urea solutions. In general, at comparable molalities, urea decreases T_m for each transition to a greater extent than does glycine betaine.

Since all three transitions are evident in the first-derivative UV-absorbance melting curves at all cosolute and NaCl molalities studied with only a moderate change in enthalpy, with the exception of the isostabilizing ability of glycine betaine, there is little evidence of a structural change in the folded ΔU177 pseudoknot structure in the presence of glycine betaine or urea. Also, Table 2 of the Supporting Information provides sequential transition fitting parameters A_i^{260} and A_i^{280} for the ΔU177 pseudoknot at each cosolute and NaCl molality. Given standard errors for the A_i^{260} and A_i^{280} fitting parameters, the near constancy of these parameters for each unfolding transition indicates the cosolutes cause little, if any, structural change in the RNA pseudoknot. Circular dichroism (*15*) and UV-absorbance thermal denaturation (*12*, *13*) have also been used to show that urea simply lowers RNA melting temperatures without altering the unfolding transitions.

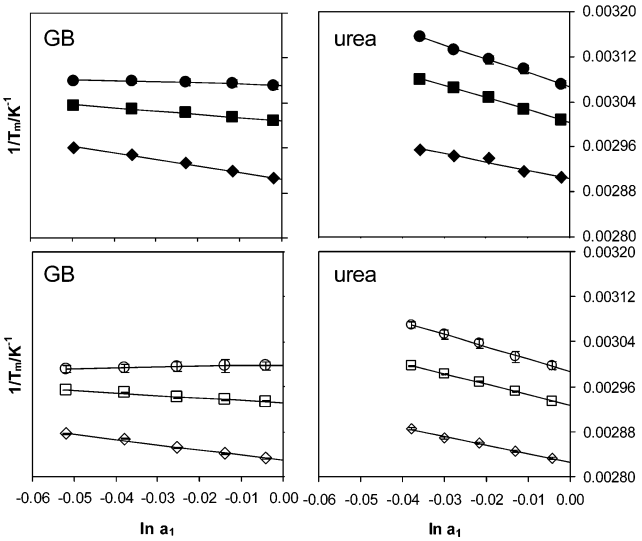

FIGURE 3: Inverse melting temperatures (T_m^{-1}) as a function of the natural logarithm of water activity (ln a_1) for the ΔU177 hTR pseudoknot in 40 m*m* NaCl (filled symbols) and 135 m*m* NaCl (empty symbols) solutions containing either glycine betaine (GB) or urea. Tertiary (loop 1 and loop 2) unfold (○,●), stem 2 unfold (□,■), and stem 1 unfold (◇,◆).

Quantitation of ΔU177 hTR Pseudoknot Unfolding with $\Delta\Gamma_{\mu_3,m_4}/m_3$. The dependence of $1/T_m$ on water activity a_1 is plotted in Figure 3 for the ΔU177 pseudoknot in glycine betaine and urea solutions at 40 and 135 m*m* NaCl. Linear regression of the plots in Figure 3 yields $dT_m^{-1}/d(\ln a_1)$ for each pseudoknot transition, which can be used with eq 4 to yield the molality-normalized change in preferential interaction coefficients $\Delta\Gamma_{\mu_3,m_4}/m_3$. In eq 4, we use the enthalpy data in Table 1 for cosolute-free solutions to determine values of $\Delta\Gamma_{\mu_3,m_4}/m_3$ in Table 2. Since $\Delta H^\circ_{T_m}$ is dependent on cosolute concentration, values of $\Delta\Gamma_{\mu_3,m_4}/m_3$ in Table 2 can be regarded as limiting values as the concentration of cosolute approaches zero ($m_3 \rightarrow 0$).

As far as we know, only the temperature dependence of the preferential interaction of urea with the *lac* repressor has been studied (*38*). Temperature correction of $\Delta\Gamma_{\mu_3,m_4}/m_3$ in Table 2 to 35 °C using the urea-*lac* repressor $\Delta\Gamma_{\mu_3,m_4}/m_3$ temperature dependence (*38*) yields a 2−10% increase in $\Delta\Gamma_{\mu_3,m_4}/m_3$ for the RNA secondary and tertiary structures studied in this work, since the preferential interaction of urea is enthalpically driven (*38*). However, the ΔASA-normalized temperature-corrected $\Delta\Gamma_{\mu_3,m_4}/m_3$ data and the temperature-uncorrected $\Delta\Gamma_{\mu_3,m_4}/m_3$ values in Table 2 scale identically

Table 2: Change in Preferential Interaction Coefficients, $\Delta\Gamma_{\mu_3,m_4}/m_3$, and the Number of Waters Released, Δn_1, in Glycine Betaine (GB) and Urea Solutions for Unfolding of the ΔU177 hTR Pseudoknot and p2b hTR Hairpin Secondary and Tertiary Structures[a]

	ΔU177 tertiary		ΔU177 stem 2		ΔU177 stem 1		p2b uridine helix and pentaloop		p2b stem 1	
	Δn_1	$\Delta\Gamma_{\mu_3,m_4}/m_3$ (m^{-1})	Δn_1	$\Delta\Gamma_{\mu_3,m_4}/m_3$ (m^{-1})	Δn_1	$\Delta\Gamma_{\mu_3,m_4}/m_3$ (m^{-1})	Δn_1	$\Delta\Gamma_{\mu_3,m_4}/m_3$ (m^{-1})	Δn_1	$\Delta\Gamma_{\mu_3,m_4}/m_3$ (m^{-1})
					40 m*m* NaCl					
GB	3.6 ± 0.8	0.065 ± 0.014	24.2 ± 1.8	0.435 ± 0.032	30.8 ± 1.4	0.554 ± 0.026	5.1 ± 0.8	0.091 ± 0.015	30.2 ± 1.3	0.544 ± 0.023
urea	42.9 ± 2.1	0.773 ± 0.037	91.2 ± 2.8	1.64 ± 0.05	38.9 ± 4.4	0.701 ± 0.080	49.6 ± 1.3	0.892 ± 0.023	40.1 ± 2.4	0.721 ± 0.043
					135 m*m* NaCl					
GB	−2.0 ± 0.3	−0.037 ± 0.006	18.8 ± 1.4	0.338 ± 0.025	25.2 ± 1.5	0.454 ± 0.028	3.6 ± 1.1	0.064 ± 0.020	25.7 ± 1.1	0.463 ± 0.020
urea	37.8 ± 1.8	0.681 ± 0.032	80.5 ± 2.2	1.45 ± 0.04	40.6 ± 1.9	0.732 ± 0.035	41.8 ± 1.8	0.753 ± 0.033	42.0 ± 0.3	0.755 ± 0.006

[a] All RNA/cosolute solutions were prepared in a 10 mM sodium phosphate buffer (pH 7.0).

Table 3: Change in Accessible Surface Area (ΔASA) for Unfolding of the ΔU177 hTR Pseudoknot and p2b hTR Hairpin Secondary and Tertiary Structures[a]

	ΔASA (Å^2)	anionic ΔASA (Å^2)[b]	amide ΔASA (Å^2)[b]	other polar ΔASA (Å^2)[b]	nonpolar ΔASA (Å^2)[b]
ΔU177 pseudoknot tertiary structure	3316	529 (16%)	651 (20%)	1104 (33%)	1032 (31%)
ΔU177 pseudoknot stem 2	1819	−72 (−4.0%)	650 (36%)	822 (45%)	420 (23%)
ΔU177 pseudoknot stem 1	1178	−91 (−7.7%)	493 (42%)	542 (46%)	234 (20%)
p2b hairpin uridine helix and pentaloop	1560	−103 (−6.6%)	894 (57%)	323 (21%)	446 (29%)
p2b hairpin stem 1	1297	−85 (−6.5%)	538 (42%)	587 (45%)	257 (20%)
p2b hairpin uridine helix	1158	−69 (−6.0%)	686 (59%)	246 (21%)	296 (26%)

[a] Unfolded nucleotides in a half-stacked conformation. [b] Anionic, amide, other polar, and nonpolar ΔASA definitions from Hong et al. (*22*).

with the fraction of polar amide ΔASA (see the Discussion and Figure 7). Thus, since no data for the temperature dependence of the preferential interaction of glycine betaine with a biopolymer surface that would allow us to correct our $\Delta\Gamma_{\mu_3,m_4}/m_3$ values exist and we obtain identical surface area analysis results using temperature-corrected or uncorrected urea $\Delta\Gamma_{\mu_3,m_4}/m_3$ values, the $\Delta\Gamma_{\mu_3,m_4}/m_3$ values in Table 2 remain uncorrected for temperature.

Urea is a significantly stronger RNA denaturant than glycine betaine as quantified by the stronger dependence of the T_ms for the unfolding transitions on water activity in urea solutions (Figure 3). Except for the tertiary unfold in glycine betaine solutions at 135 m*m* NaCl, $\Delta\Gamma_{\mu_3,m_4}/m_3$ is positive (Table 2), indicating accumulation of glycine betaine and urea at the newly exposed surfaces of unfolded RNA secondary and tertiary structures. Increasing the NaCl concentration from 40 to 135 m*m* lowers $\Delta\Gamma_{\mu_3,m_4}/m_3$ values for the unfolding transitions, attenuating the interaction of glycine betaine and urea with the newly exposed surface area of unfolded RNA. For the tertiary transition in 135 m*m* NaCl, glycine betaine actually acts as a stabilizing agent, increasing T_m with increasing glycine betaine molality (Figure 3). The attenuation of $\Delta\Gamma_{\mu_3,m_4}/m_3$ with an increasing ionic strength has been observed with dsDNA melting and has been attributed to the dependence of cosolute accumulation at the newly exposed unfolded surfaces on salt concentration and counterion release (*11*). The weak interaction of glycine betaine with the newly exposed surface area in the tertiary unfold, as quantified by $\Delta\Gamma_{\mu_3,m_4}/m_3$ in Table 2, is presumably due to the exclusion of glycine betaine from anionic oxygens exposed during the tertiary unfolding process (see Table 3) (*39*).

p2b hTR Hairpin. The p2b hTR hairpin unfolds in two sequential transitions corresponding to the U-rich helix and pentaloop followed by GC-rich stem 1 (Figure 1) (*18*). Figure 4 shows representative p2b hairpin 260 and 280 nm first-derivative UV-absorbance melting curves in glycine betaine and urea solutions at 135 m*m* NaCl. As with the ΔU177 pseudoknot, the two transitions in the p2b hairpin were reversible, although the RNA underwent degradation at high temperatures. Thus, p2b hairpin samples were thermally unfolded once before being discarded.

Table 1 lists the melting temperatures and enthalpy changes predicted for sequential unfolding of the p2b hairpin uridine helix and pentaloop and stem 1 in cosolute-free solutions at 40 and 135 m*m* NaCl. A table listing melting temperatures and enthalpy changes for the p2b hairpin uridine helix and pentaloop and stem 1 at all cosolute molalities can be found in the Supporting Information. Additionally, Table 3 of the Supporting Information provides A_i^{260} and A_i^{280} fitting parameters for the p2b hairpin at all cosolute and sodium chloride molalities. As with the pseudoknot, no detectable patterns in A_i^{260} and A_i^{280} are evident (given standard errors) with cosolute concentration, indicating the cosolutes have little, if any, effect on hairpin structure. However, the A_i^{260} and A_i^{280} parameters for the p2b uridine helix and pentaloop are larger in 135 m*m* NaCl with glycine betaine. The enhancement in the total UV absorption change for the uridine helix may reflect a slight increase in the degree of folding relative to that without glycine betaine.

As seen in Figures 2 and 4 and Table 1, T_m is lower for stem 1 in the p2b hairpin than in the ΔU177 pseudoknot, although $\Delta H^\circ_{T_m}$ remains essentially unchanged (Table 1). Our measured T_m for p2b stem 1 in 135 m*m* NaCl is in good agreement with stem 1 melting in 200 mM KCl for both the wild-type hTR pseudoknot containing the U177 bulge and the p2b hairpin (*18*). The larger T_m of stem 1 in the ΔU177 pseudoknot is presumably due to a smaller entropy gain for unfolding given the different local environments for stem 1 in the pseudoknot and hairpin RNA structures (*17, 18*).

As with the ΔU177 pseudoknot, glycine betaine destabilizes GC-rich stem 1 more so than any other secondary structure. As shown in Figure 4, the two transitions begin to coalesce into a single transition due to isostabilization in 2 *m* glycine betaine. Even with glycine betaine's isostabiliza-

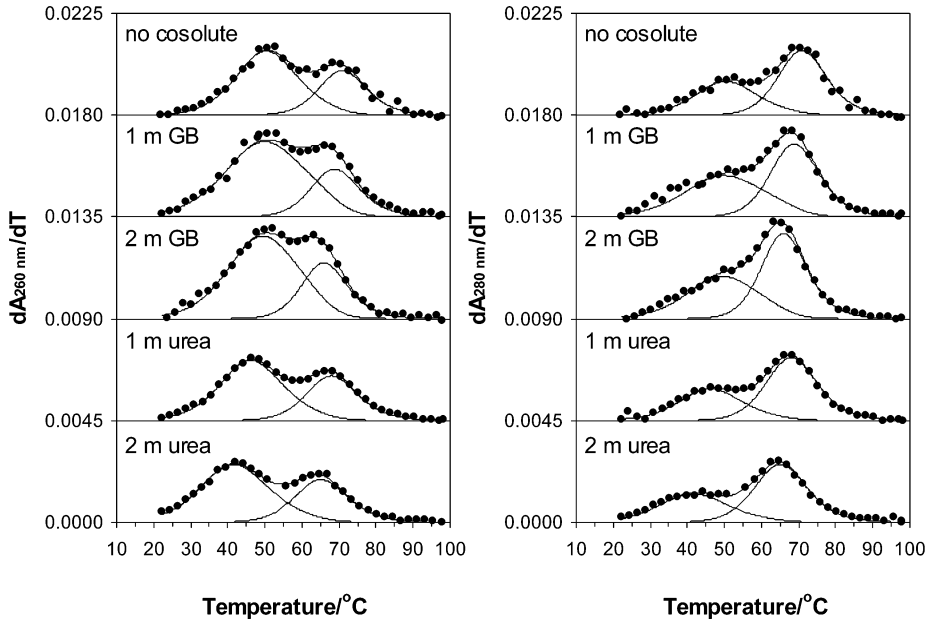

FIGURE 4: Absorbance first-derivative melting profiles at 260 and 280 nm for 2.25 μM p2b hTR hairpin in 135 m*m* NaCl solutions containing either glycine betaine (GB) or urea. Composite fits (solid lines) are superimposed on the experimental data (every eleventh data point shown). The two individual transitions of the composite fit are shown as solid lines. Curves are offset on the *y*-axes to illustrate trends in peak position with added cosolute.

tion effect on the T_ms of the p2b hairpin uridine helix and pentaloop and stem 1, $\Delta H^\circ_{T_m}$ remains largely unaffected (see the Supporting Information). Urea destabilizes the p2b hairpin to a greater extent than glycine betaine (Figure 4). Both transitions are shifted to lower temperatures in urea solutions than those in glycine betaine solutions. Enthalpies of unfolding remain essentially unchanged with urea; values of $\Delta H^\circ_{T_m}$ for the transitions are attenuated at most by 7% in 2 *m* urea (see the Supporting Information).

Figure 5 plots the dependence of $1/T_m$ on water activity a_1 for the p2b hairpin in glycine betaine and urea solutions at 40 and 135 m*m* NaCl. Table 2 lists values of $\Delta\Gamma_{\mu_3,m_4}/m_3$ and Δn_1 for the U-rich helix and pentaloop and stem 1 obtained from linear regression of the plots in Figure 5. Values of $\Delta\Gamma_{\mu_3,m_4}/m_3$ and Δn_1 for stem 1 in the p2b hairpin and ΔU177 pseudoknot are statistically identical within experimental error. Interaction of glycine betaine with the uridine helix and pentaloop is weak, which is not surprising given the preference of glycine betaine for GC-rich RNA duplexes.

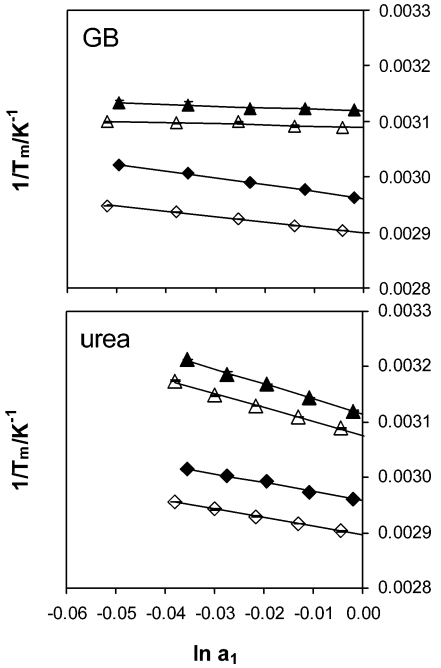

FIGURE 5: Inverse melting temperatures (T_m^{-1}) as a function of the natural logarithm of water activity (ln a_1) for the p2b hTR hairpin in 40 m*m* NaCl (filled symbols) and 135 m*m* NaCl (empty symbols) solutions containing either glycine betaine (GB) or urea. Uridine helix and pentaloop unfold (△,▲) and stem 1 unfold (◇,◆).

DISCUSSION

Preferential Interaction of Glycine Betaine and Urea with the ΔU177 hTR Pseudoknot and p2b Hairpin. For dsDNA in a 5 mM sodium phosphate buffer with no added NaCl, plots of $1/T_m$ versus the natural logarithm of a_1 in glycine betaine solutions were concave downward, indicating a nonconstant $\Delta\Gamma_{\mu_3,m_4}/m_3$ (*11*). However, this curvature was not apparent with added NaCl and was not observed with the RNA experiments in this work.

Similar to dsDNA melting (*7*, *11*), glycine betaine has the strongest interaction (largest $\Delta\Gamma_{\mu_3,m_4}/m_3$ in Table 2) with the GC-rich ΔU177 pseudoknot and p2b hairpin stem 1. For dsDNA with 72% GC content and no added NaCl, $\Delta\Gamma_{\mu_3,m_4}/m_3$ (per base pair) at 1 *m* glycine betaine was 0.12 ± 0.01 m^{-1} (*11*), which compares favorably with the $\Delta\Gamma_{\mu_3,m_4}/m_3$ of 0.091 ± 0.004 m^{-1} (per base pair) in 40 m*m* NaCl for stem 1 (83% GC, 6 bp) in the ΔU177 pseudoknot and p2b hairpin (Table 2). Nordstrom et al. (*11*) found $\Delta\Gamma_{\mu_3,m_4}/m_3$ (per base pair) for 42% GC dsDNA at 1 *m* glycine betaine to be 0.039 ± 0.006 and 0.030 ± 0.006 m^{-1} in 50 and 150 m*m* NaCl, respectively. For ΔU177 pseudoknot stem 2 studied in this work (44% GC, 9 bp), $\Delta\Gamma_{\mu_3,m_4}/m_3$ = 0.048 ± 0.004 and 0.038 ± 0.004 m^{-1} (per base pair) in 40 and 135 m*m* NaCl, respectively (Table 2). Values of $\Delta\Gamma_{\mu_3,m_4}/m_3$ for dsDNA, stem 2, and stem 1 at similar salt concentrations and GC content are nearly indistinguishable given experimental errors. Thus,

we propose a similar mechanism of interaction exists between glycine betaine and the surface area exposed in dsDNA and RNA base pair unfolding.

Urea has the strongest interaction with the surface area exposed in unfolding AU-rich ΔU177 pseudoknot stem 2, as with AT-rich dsDNA (*9*, *11*). For stem 2, $\Delta\Gamma_{\mu_3,m_4}/m_3$ (per base pair) = 0.182 ± 0.006 and 0.161 ± 0.004 m^{-1} in 40 and 135 m*m* NaCl, respectively (Table 2). These interaction parameters are statistically larger than those for 42% GC dsDNA ($\Delta\Gamma_{\mu_3,m_4}/m_3$ = 0.109 ± 0.002 and 0.089 ± 0.005 m^{-1} at 50 and 150 m*m* NaCl, respectively) (*11*). For the ΔU177 pseudoknot and p2b hairpin stem 1, $\Delta\Gamma_{\mu_3,m_4}/m_3$ = 0.118 ± 0.011 m^{-1} (per base pair) in 40 m*m* NaCl (Table 2). In comparison, $\Delta\Gamma_{\mu_3,m_4}/m_3$ = 0.093 ± 0.010 m^{-1} (per base pair) for 72% GC dsDNA in the absence of NaCl (*11*). Unlike glycine betaine, urea has a slightly stronger interaction per base pair with RNA double-helical segments than dsDNA at similar salt concentrations and GC contents. However, the ratio $(\Delta\Gamma_{\mu_3,m_4}/m_3)_{\text{stem 2}}/(\Delta\Gamma_{\mu_3,m_4}/m_3)_{\text{stem 1}}$ = 1.56 in 40 m*m* NaCl and the ratio $(\Delta\Gamma_{\mu_3,m_4}/m_3)_{42\%\text{ GC dsDNA}}/(\Delta\Gamma_{\mu_3,m_4}/m_3)_{72\%\text{ GC dsDNA}}$ = 1.55 with no added NaCl indicate a similar enhancement of urea accumulation at the newly exposed unfolded bases with decreasing dsDNA and duplex RNA GC content. Whether the presence of uracil in RNA, which lacks the hydrophobic methyl group of thymine, or the ribose sugar in RNA and the A-conformation of stems 2 and 1 account for these observations is unclear.

Interestingly, values of $\Delta\Gamma_{\mu_3,m_4}/m_3$ (per base pair) are larger for interaction of urea with stem 2 in the ΔU177 pseudoknot than the U-rich helix of the p2b hairpin. To illustrate, in urea solutions at 40 m*m* NaCl, $\Delta\Gamma_{\mu_3,m_4}/m_3$ = 0.182 ± 0.006 for stem 2 and 0.149 ± 0.004 (per base pair) for the U-rich helix and pentaloop. Accumulation of urea at a biopolymer surface is directly proportional to the number of solvent-accessible ASA amide functional groups (*15*, *22*). Despite the greater number of amide functional groups exposed upon unfolding the uridine helix and pentaloop (Table 3), urea has more favorable interaction with the surface area exposed during stem 2 thermal denaturation. The preference of urea for the newly exposed surface area of stem 2 suggests a significant role for adenine in urea nucleic acid destabilization. However, the ΔU177 pseudoknot and p2b hairpin stem 1 and the uridine helix contain an equal number of base pairs. As expected, $\Delta\Gamma_{\mu_3,m_4}/m_3$ is larger for the p2b hairpin uridine helix and pentaloop than that for stem 1 because of its larger amide ΔASA (Table 3).

It should be noted that positive values of $\Delta\Gamma_{\mu_3,m_4}/m_3$ do not guarantee accumulation of glycine betaine and urea at the unfolded RNA secondary and tertiary structures relative to bulk solution. Since $\Delta\Gamma_{\mu_3,m_4}/m_3$ represents a change in $\Gamma_{\mu_3,m_4}/m_3$ between unfolded and folded RNA secondary and tertiary structures, exclusion of cosolute from the unfolded biopolymer ($\Gamma_{\mu_3,m_4}/m_3 < 0$) can still generate a positive $\Delta\Gamma_{\mu_3,m_4}/m_3$ as long as $\Gamma^{\text{unfolded}}_{\mu_3,m_4} > \Gamma^{\text{folded}}_{\mu_3,m_4}$ (*11*). Glycine betaine is generally excluded ($\Gamma^{\text{folded}}_{\mu_3,m_4} < 0$) from the surfaces of protein (*23*, *25*, *39*−*41*) and dsDNA native structures (*22*), presumably due to exclusion of glycine betaine from solvent-accessible anionic oxygens (*39*). In addition, urea accumulates at amide functional groups (*15*, *22*) and is neither accumulated nor excluded from the vicinity of salt ions (K^+, Na^+, and Cl^-) (*42*) and the anionic oxygens of dsDNA (*22*). Thus, in contrast to glycine betaine, urea is mildly accumulated ($\Gamma^{\text{folded}}_{\mu_3,m_4} > 0$) at folded protein surfaces (*4*, *41*) and shows no preferential accumulation or exclusion ($\Gamma^{\text{folded}}_{\mu_3,m_4} \approx 0$) at the dsDNA surface (*22*). However, positive values of $\Delta\Gamma_{\mu_3,m_4}/m_3$ do at least indicate accumulation of glycine betaine and urea at the newly exposed RNA surface upon unfolding relative to bulk solution, assuming interaction of cosolute with the surface from the folded structure does not change significantly when the biopolymer unfolds. Glycine betaine is excluded and urea not preferentially accumulated or excluded from 42% GC dsDNA surfaces in 200 m*m* KCl solutions (*22*). If similar behavior exists for double-helical RNA, positive values of $\Delta\Gamma_{\mu_3,m_4}/m_3$ indicate less exclusion of glycine betaine from unfolded stems 2 and 1 relative to the folded stems and accumulation of urea at these unfolded RNA duplexes relative to bulk solution.

ΔU177 hTR Pseudoknot and p2b Hairpin Hydration. The conformation of folded RNA structures is intimately tied to hydration. In general, formation of nucleic acid duplexes and triplexes results in an uptake of hydrating waters (*30*, *43*−*48*). Using eq 5, we estimated the number of waters released per unfolding transition, Δn_1, for the ΔU177 pseudoknot and p2b hairpin (see Table 2). The change in the number of hydrating waters probed in this manner is generally assigned to waters uniquely bound within duplex or triplex nucleic acid structures and most importantly in the conformation and stability of these structures (*30*). However, the Δn_1 and $\Delta\Gamma_{\mu_3,m_4}/m_3$ values are intimately related; accumulation of cosolute necessarily means an exclusion or release of water.

The weak interaction of glycine betaine with the newly exposed surface area for unfolding the tertiary structure of the ΔU177 pseudoknot (as characterized by $\Delta\Gamma_{\mu_3,m_4}/m_3$ in Table 2) results in approximately four waters released in 40 m*m* NaCl and an uptake of two waters in 135 m*m* NaCl. In contrast, the high affinity of urea for the unfolded tertiary structure results in a 10-fold greater number of waters released during the unfolding transition as compared to glycine betaine. The positions of loop 1 in the major groove of stem 2 and loop 2 in the minor groove of stem 1 in the ΔU177 pseudoknot suggest a substantive number of these waters originate from the grooves formed on either side of the loops. For DNA triplexes, NMR (*47*) and molecular dynamics (*45*) suggest only a small number of water molecules in triplex grooves. The tertiary structure of the pseudoknot does contain triplexes. U100−U102 are involved in Hoogsteen base triples with U115-A174, U114-A175, and U113-A176 Watson−Crick base pairs. A172 forms a base triple with the C116-G98 base pair, and there is evidence of a hydrogen bond between A171 and the A117-U97 base pair (*17*). While hydration patterns between triplex DNA and the pseudoknot tertiary structure are most likely different to some extent, the small number of waters released in glycine betaine and urea solutions (per loop 1 and 2 bases) for the pseudoknot tertiary unfold is consistent with similar nucleic acid structures.

Values of Δn_1 in Table 2 for stems 1 and 2 and the p2b hairpin uridine helix and pentaloop reflect the different affinity of glycine betaine and urea for GC-rich RNA duplexes. In 40 m*m* NaCl, unfolding the RNA duplexes in glycine betaine solutions results in 2.7 ± 0.2 waters released per stem 2 base pair and 5.1 ± 0.2 waters released per stem

1 base pair. These values are attenuated by approximately 20% in 135 m*m* NaCl. These values of Δn_1 are comparable to those for 42% GC dsDNA (3.1 ± 0.5 waters per base pair) and 72% GC dsDNA (6.7 ± 0.6 waters per base pair) at 1 *m* glycine betaine in a 5 mM sodium phosphate buffer (*11*), although B-form DNA is generally thought to be more hydrated than A-form RNA (*43*). However, the stronger affinity of urea for unfolded stems 1 and 2 results in a greater level of dehydration of the RNA duplexes upon unfolding. In 40 m*m* NaCl, unfolding the RNA duplexes in urea solutions releases 10.1 ± 0.3 waters per stem 2 base pair and 6.6 ± 0.6 waters per stem 1 base pair. These numbers are statistically larger than those for 42% GC dsDNA (8.0 ± 0.1 waters per base pair) and 72% GC dsDNA (5.2 ± 0.6 waters per base pair) in 5 mM sodium phosphate buffer (*11*). While glycine betaine and urea do exhibit different affinities for GC-rich RNA duplexes, Δn_1 values are in general agreement with the five to eight waters specifically bound in AU and GC major and minor grooves (*48*).

In contrast to that of stems 1 and 2, the weak interaction of glycine betaine with the unfolded p2b uridine helix results in approximately one water released per base pair (Table 2). In contrast, the high affinity of urea for the amide-rich surface area exposed upon unfolding the uridine helix releases approximately eight waters per base pair.

Interaction of Glycine Betaine with Unfolded RNA Correlates with the Fraction of Nonpolar ΔASA. Values of $\Delta\Gamma_{\mu_3,m_4}/m_3$ for glycine betaine in Table 2 indicate glycine betaine can distinguish between all four unique structures in the ΔU177 pseudoknot and p2b hairpin: the pseudoknot tertiary structure, AU-rich stem 2, GC-rich stem 1, and the uridine helix and pentaloop. Glycine betaine actually stabilizes the tertiary structure of the ΔU177 pseudoknot in 135 m*m* NaCl just as it does for protein tertiary structure. This marks the second case where a cosolute can actually stabilize the tertiary structure of RNA, the first being TMAO's ability to counteract urea destabilization of the tertiary structure of $tRNA^{fmet}$ (*12*).

To identify a unifying trend in glycine betaine's interaction with these distinct RNA structures, we have determined ΔASA values for unfolding each of the pseudoknot and hairpin secondary and tertiary structures (Table 3). In our calculations, we assumed that the structural elements of the pseudoknot and hairpin unfold sequentially and that each structural unit contributes only to the assigned transitions. As a check of our calculations, we can make comparisons to dsDNA ΔASA calculations. Although dsDNA and RNA duplexes have different conformations, most of the chemical functional groups exposed are essentially the same. In the half-stacked model for unfolding the dsDNA helix, the fractional change in anionic oxygen ΔASA is −7% since phosphate groups become occluded as base stacking is disrupted (*22*). We calculate the fractional change in anionic oxygen ΔASA for stem 1 in the pseudoknot and hairpin and the U-rich helix and pentaloop to be approximately −7% (Table 3), in good agreement with dsDNA half-stacked unfolding. The estimate for the stem 2 fraction anionic oxygen ΔASA is −4%, lower than that determined for the other RNA secondary structures. In the determination of the ΔASA for the stems in the pseudoknot, loop 1 bases 100−105 and loop 2 bases 167−173 were excised before the ASA of the folded stems was calculated. To minimize end effects, the initial and terminal bases from the loops were left intact on the folded stems, since these loop anchor points are expected to be in or near their current positions even when loops 1 and 2 are denatured. C106 of loop 1 was left buried in the major groove of stem 2 which occludes some anionic oxygen ASA and accounts for the slightly lower fraction of anionic oxygen ΔASA for stem 2. From these observations, we estimate a 1−2% error in our double-helical RNA ΔASA calculations based on the position uncertainty of the initial and terminal bases of the denatured loops. Our estimates for fraction amide, other polar, and nonpolar ΔASA values in Table 3 are in good agreement with those determined for 50% GC dsDNA (*22*), with almost identical results for stem 2 (44% GC content). However, the unfolding of the tertiary structure of the ΔU177 pseudoknot is ambiguous. Our description of the pseudoknot tertiary unfold takes the ASA of the half-stacked unfolded pseudoknot and subtracts both the ASA of the folded pseudoknot and the ASA of stems 1 and 2 with the loops excised. Thus, our description of the pseudoknot tertiary unfold contains only the ΔASA from exposing the buried surface area of the loops and the minor groove of stem 1 and the major groove of stem 2.

For comparisons of $\Delta\Gamma_{\mu_3,m_4}/m_3$ for the interaction of glycine betaine with the different RNA secondary and tertiary structures in the pseudoknot and hairpin, $\Delta\Gamma_{\mu_3,m_4}/m_3$ values in Table 2 were normalized by ΔASA for the unfolding transitions. These ΔASA-normalized preferential interaction coefficients, $\Delta\Gamma_{\mu_3,m_4}/(m_3\Delta\text{ASA})$, provide a quantitative measure of the interaction of glycine betaine with one unit area (1 Å^2) of the unfolded surface (*39*). Felitsky et al. (*39*) have demonstrated that glycine betaine is excluded from the water-accessible surface area of anionic oxygens. However, in our ΔASA calculations, except for the tertiary pseudoknot unfold, the fractions of anionic oxygen ΔASA for stem 1, stem 2, and the U-rich helix and pentaloop are almost identical. Thus, exclusion of glycine betaine from anionic oxygens does not account for the preferential interaction of glycine betaine with these RNA secondary structures. We observe that $\Delta\Gamma_{\mu_3,m_4}/(m_3\Delta\text{ASA})$ correlates most strongly with the fraction of nonpolar ΔASA. Figure 6 plots $\Delta\Gamma_{\mu_3,m_4}/(m_3\Delta\text{ASA})$ as a function of the fraction of nonpolar ΔASA and shows that the enhanced level of accumulation of glycine betaine at unfolded RNA secondary and tertiary structures relative to the folded structures decreases linearly with the fraction of nonpolar ΔASA.

If we consider $\Delta\Gamma_{\mu_3,m_4}/(m_3\Delta\text{ASA})$ a weighted sum of all the $\Delta\Gamma_{\mu_3,m_4}/(m_3\Delta\text{ASA})_{100\%\text{i}}$ values for a 100% surface area of type i (i = anionic oxygen, amide, other polar, or nonpolar), we can write

$$\Delta\Gamma_{\mu_3,m_4}/(m_3\Delta\text{ASA}) = \sum_{\text{i}} \Delta\Gamma_{\mu_3,m_4}/(m_3\Delta\text{ASA})_{100\%\,\text{i}} f_{\text{i}} \quad (6)$$

where f_{i} is the fraction of type i ΔASA. Linear regression of the data in Figure 6 yields the following slopes: $10^3 \times \Delta\Gamma_{\mu_3,m_4}/(m_3\Delta\text{ASA})_{100\%\ \text{nonpolar}} = -3.9 \pm 0.5$ and -3.4 ± 0.4 m^{-1}/Å^2 in 40 and 135 m*m* NaCl, respectively. The $10^3 \times \Delta\Gamma_{\mu_3,m_4}/(m_3\Delta\text{ASA})_{0\%\ \text{nonpolar}}$ intercepts equal 1.2 ± 0.1 and 1.0 ± 0.1 m^{-1}/Å^2 in 40 and 135 m*m* NaCl, respectively, and reflect contributions to $\Delta\Gamma_{\mu_3,m_4}/(m_3\Delta\text{ASA})$ from the other types of surfaces exposed for unfolding RNA secondary and tertiary structure. Exclusion of glycine betaine from nonpolar

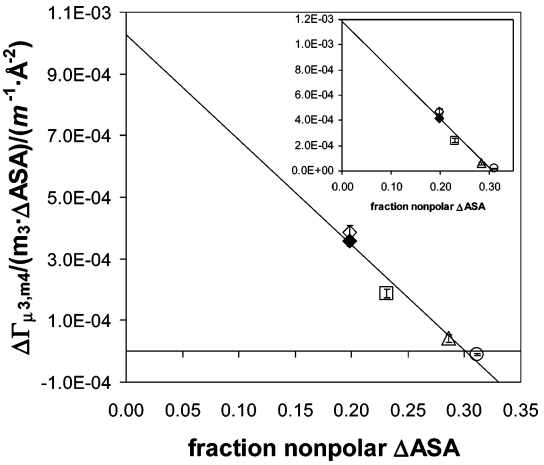

FIGURE 6: Accumulation of glycine betaine characterized by $\Delta\Gamma_{\mu_3,m_4}/(m_3\Delta\text{ASA})$ at the surface area exposed upon unfolding (ΔASA) the ΔU177 hTR pseudoknot and p2b hTR hairpin secondary and tertiary structures as a function of the fraction of nonpolar ΔASA in 135 m*m* NaCl. ΔU177 pseudoknot loop 1 − loop 2 tertiary fold (○), stem 2 (□), stem 1 (◇). p2b hairpin uridine helix and pentaloop (△) and stem 1 (◆). The inset is for 40 m*m* NaCl. Linear regression yields a $10^3 \times \Delta\Gamma_{\mu_3,m_4}/(m_3\Delta\text{ASA})$ value of $(1.0 \pm 0.1) - (3.4 \pm 0.4)f_{\text{nonpolar }\Delta\text{ASA}}$ for 135 m*m* NaCl and a $10^3 \times \Delta\Gamma_{\mu_3,m_4}/(m_3\Delta\text{ASA})$ value of $(1.2 \pm 0.1) - (3.9 \pm 0.5)f_{\text{nonpolar }\Delta\text{ASA}}$ for 40 m*m* NaCl.

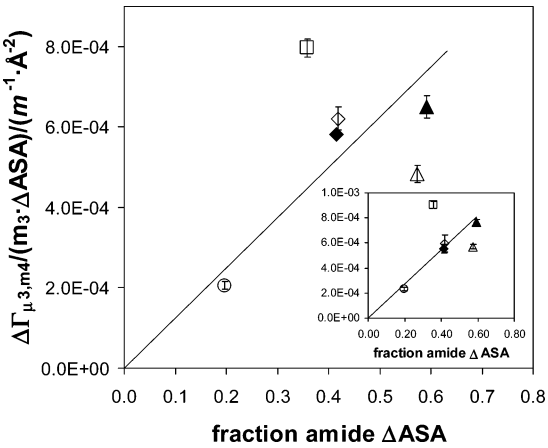

FIGURE 7: Accumulation of urea characterized by $\Delta\Gamma_{\mu_3,m_4}/(m_3\Delta\text{ASA})$ at the surface area exposed upon unfolding (ΔASA) the ΔU177 hTR pseudoknot and p2b hTR hairpin secondary and tertiary structures as a function of the fraction of amide ΔASA in 135 m*m* NaCl. ΔU177 pseudoknot loop 1 − loop 2 tertiary fold (○), stem 2 (□), and stem 1 (◇). p2b hairpin uridine helix and pentaloop (△) and stem 1 (◆). Due to potential uncertainty in determining the ΔASA of the uridine helix and pentaloop unfold, $\Delta\Gamma_{\mu_3,m_4}/(m_3\Delta\text{ASA})$ is also plotted for the uridine helix and pentaloop unfold using the ΔASA for the uridine helix only (▲). This datum was not used in the linear regression. The inset is for 40 m*m* NaCl. Linear regression yields a $10^3 \times \Delta\Gamma_{\mu_3,m_4}/(m_3\Delta\text{ASA})$ value of $(1.3 \pm 0.2)f_{\text{amide}\Delta\text{ASA}}$ for 135 m*m* NaCl and a $10^3 \times \Delta\Gamma_{\mu_3,m_4}/(m_3\Delta\text{ASA})$ value of $(1.4 \pm 0.3)f_{\text{amide }\Delta\text{ASA}}$ for 40 m*m* NaCl.

surfaces necessarily indicates accumulation at polar surfaces exposed upon unfolding. Increasing ionic strength attenuates both accumulation of glycine betaine at polar chemical functional groups that have favorable interaction with glycine betaine as well as exclusion from nonpolar surfaces. While $\Delta\Gamma_{\mu_3,m_4}/(m_3\Delta\text{ASA})$ is an increasing function of the fraction polar ΔASA as expected, the correlation is poorer than the correlation with the fraction nonpolar ΔASA; the p2b hairpin uridine helix and pentaloop have a significantly smaller $\Delta\Gamma_{\mu_3,m_4}/(m_3\Delta\text{ASA})$ than would be expected given its high fraction of polar ΔASA. This result is presumably due to exclusion of glycine betaine from the large polar amide ΔASA exposed in the uridine helix (*39*). We find that exclusion of glycine betaine from a nonpolar surface is quite strong, only slightly less than $10^3 \times \Delta\Gamma_{\mu_3,m_4}/(m_3\Delta\text{ASA})_{100\%\text{ anionic oxygen}} = -4.0 \pm 0.3\ m^{-1}/\text{Å}^2$ anticipated for exclusion of glycine betaine from anionic oxygens (*39*). Additionally, Felitsky et al. (*39*) have shown glycine betaine to be strongly excluded from polar amide surfaces as determined by a two-parameter analysis of anionic oxygen and amide surface areas. We found little correlation of $\Delta\Gamma_{\mu_3,m_4}/(m_3\Delta\text{ASA})$ with the fraction of amide ΔASA; glycine betaine has a stronger preference for GC-rich stem 1 [larger $\Delta\Gamma_{\mu_3,m_4}/(m_3\Delta\text{ASA})$] than stem 2 despite stem 1's higher fraction of amide ΔASA. Additionally, despite its low fraction of amide ΔASA, the pseudoknot tertiary unfold exposes a significant amount of anionic oxygen ASA. However, $\Delta\Gamma_{\mu_3,m_4}/(m_3\Delta\text{ASA})$ for the p2b hairpin U-rich helix and pentaloop is smallest, presumably because of its large fraction of amide ΔASA (Tables 2 and 3). The uridine helix and pentaloop manifest the largest fraction of polar amide ΔASA because of the high number of uridine bases, but also a high fraction of nonpolar ΔASA. The reason for the discrepancy between our work and that of Felitsky et al. (*39*) for glycine betaine accumulation or exclusion from amide surfaces is unclear. However, our analysis focused on biopolymer structures with a percentage of nonpolar ΔASA significantly lower than the percentage of nonpolar ASA for the lacI HTH, hen egg white lysozyme, and bovine serum albumin proteins studied by Felitsky et al. (*39*).

Why is glycine betaine excluded from nonpolar surfaces? Glycine betaine is zwitterionic at neutral pH and therefore more polar than water. Glycine betaine prefers to be hydrated by the polar solvent water, so it is not surprising the interaction between glycine betaine and the nonpolar surface area exposed on unfolding would be unfavorable. A reduction in the enhanced level of accumulation of glycine betaine near unfolded nucleic acid surfaces relative to the folded structures with increasing nonpolar character of ΔASA serves as an explanation of why GC-rich helices are destabilized more than AT- or AU-rich helices in dsDNA and RNA folded structures. However, while the decrease in the extent of exclusion of glycine betaine from unfolded RNA duplexes would be due to local accumulation of glycine betaine around unfolded bases, it is possible water organization in the RNA duplex major and minor grooves excludes glycine betaine in a sequence-dependent manner (*43*). This exclusion would be attenuated with duplex melting and the loss of the major and minor grooves.

Interaction of Urea with Unfolded AU-Rich Stem 2 Does Not Correlate with the Fraction of Amide Δ*ASA.* Urea is able to discriminate between GC-rich stem 1 and AU-rich stem 2 duplexes in the ΔU177 pseudoknot, just as it destabilizes AT-rich dsDNA more than GC-rich dsDNA (*9*, *11*). The effectiveness of urea as a biopolymer denaturant has been attributed to the strong, favorable interaction between urea and amide groups exposed upon unfolding (*22*). However, as seen in Table 3, AU-rich stem 2 actually has a smaller fraction of amide ΔASA than GC-rich stem 1. This observation is evident in Figure 7, which plots $\Delta\Gamma_{\mu_3,m_4}/(m_3\Delta\text{ASA})$ for urea as a function of the fraction of amide ΔASA. In Figure 7, $\Delta\Gamma_{\mu_3,m_4}/(m_3\Delta\text{ASA})$ for stem 2 is 33%

larger than that for stem 1, even though stem 2 has a smaller fraction of amide ΔASA. In our calculations of ΔASA, it is possible we overestimated the newly exposed surface area for the p2b uridine helix and pentaloop unfolding transition; the pentaloop's structure in solution is probably more fluid than the uridine helix. For comparison, we also plotted in Figure 7 $\Delta\Gamma_{\mu_3,m_4}/(m_3\Delta\text{ASA})$ for the uridine helix and pentaloop using the ΔASA of just the uridine helix. Most likely, the true ΔASA falls between these two extremes. This datum, however, was not used in the linear regression of the plots. Note that the small value of $\Delta\Gamma_{\mu_3,m_4}/(m_3\Delta\text{ASA})$ for the uridine helix and pentaloop in glycine betaine solutions in Figure 6 does not change significantly using just the ΔASA of the uridine helix.

In Figure 7, linear regression yields values for $10^3 \times \Delta\Gamma_{\mu_3,m_4}/(m_3\Delta\text{ASA})_{100\%\text{ amide}}$ of 1.4 ± 0.3 and 1.3 ± 0.2 m^{-1}/Å^2 in 40 and 135 m*m* NaCl, respectively. These values are in good agreement with the $10^3 \times \Delta\Gamma_{\mu_3,m_4}/(m_3\Delta\text{ASA})_{100\%\text{ amide}}$ value of 1.62 ± 0.07 m^{-1}/Å^2 predicted for urea accumulation at dsDNA and protein surfaces (*22*). The zero intercept in Figure 7 indicates that any contribution to $\Delta\Gamma_{\mu_3,m_4}/(m_3\Delta\text{ASA})$ from interaction of urea with other surface types is apparently not significant compared to that for amide surfaces.

For most unfolded biopolymer surfaces, the level of urea accumulation is proportional to the number of amide functional groups in ΔASA. However, stem 2 is approximately 5−6% smaller in amide ΔASA than stem 1, yet $\Delta\Gamma_{\mu_3,m_4}/(m_3\Delta\text{ASA})$ for stem 2 is 33% larger than that for stem 1. It is unlikely that efficient packing of urea around amide-rich uridine bases in stem 2 accounts for this apparent inconsistency. The uridine helix and pentaloop structure has the largest fraction of amide ΔASA due to the large number of uridine bases, yet $\Delta\Gamma_{\mu_3,m_4}/(m_3\Delta\text{ASA})$ for the uridine helix and pentaloop is lower than that of stem 2. It is also unlikely that urea accumulation around amine-rich regions of adenine accounts for the unusually high value of $\Delta\Gamma_{\mu_3,m_4}/(m_3\Delta\text{ASA})$ for stem 2. The percentage of amine ΔASA not involved in amide groups for stem 1 and stem 2 is approximately 39 and 40%, respectively. Multiple linear regressions of $\Delta\Gamma_{\mu_3,m_4}/(m_3\Delta\text{ASA})$ with the fraction of amide ΔASA and any other surface type did not significantly improve the correlation. Whether there is actually a stronger interaction or more efficient packing of urea at unfolded AU base pairs than GC base pairs because of favorable urea−adenine interactions is unclear. Additionally, it is unknown if the preference of urea for nucleic acid duplexes is dependent on both sequence and composition. It is possible the interaction of urea with the major and minor grooves of RNA duplexes is sequence-dependent because of sequence-dependent water organization (*43*). Even if $\Gamma^{\text{unfolded}}_{\mu_3,m_4}$ is the same for all RNA duplexes, $\Gamma^{\text{folded}}_{\mu_3,m_4}$ may not be because of sequence-specific urea interactions. Experiments aimed at elucidating the mechanism of interaction of urea with AU- and AT-rich nucleic acid duplexes are currently in progress in our laboratory.

Conclusions. The interactions of the cosolutes glycine betaine and urea with the unfolded surfaces of the hTR ΔU177 pseudoknot and the hTR p2b hairpin were used to probe the secondary and tertiary structure stability of these RNAs. Glycine betaine stabilizes pseudoknot tertiary structure in 135 m*m* NaCl and shows stronger preferential interaction with unfolded GC-rich duplexes than with AU-rich duplexes. Urea destabilizes both tertiary and secondary structure and has a stronger preferential interaction with unfolded AU-rich duplexes than GC-rich duplexes. The preferential interaction of glycine betaine with unfolded secondary and tertiary RNA structures decreases as the nonpolar character of the unfolded RNA surfaces increases. Preferential interaction of urea with unfolded RNA becomes stronger with increasing amide fraction of the newly exposed unfolded surface area. However, the strong preferential interaction of urea for AU-rich duplexes relative to GC-rich duplexes is attributed to stronger preferential interaction of urea for adenine relative to guanine and cytosine bases.

ACKNOWLEDGMENT

We gratefully acknowledge the help of Olaf Hall-Holt for assistance with the T-Melt program and Linux.

SUPPORTING INFORMATION AVAILABLE

A description of the linear interpolation procedure for d*A*/d*T* baselines, thermodynamic parameters for the sequential unfolding of the ΔU177 hTR pseudoknot and p2b hTR hairpin in glycine betaine and urea solutions (Table 1), A_i^{260} and A_i^{280} sequential transition fitting parameters for the ΔU177 hTR pseudoknot and p2b hTR hairpin in glycine betaine and urea solutions (Tables 2 and 3). This material is available free of charge via the Internet at http://pubs.acs.org.

REFERENCES

1. Santoro, M. M., Liu, Y., Khan, S. M. A., Hou, L.-X., and Bolen, D. W. (1992) Increased Thermal Stability of Proteins in the Presence of Naturally Occurring Osmolytes, *Biochemistry 31*, 5278−5283.
2. Liu, Y., and Bolen, D. W. (1995) The Peptide Backbone Plays a Dominant Role in Protein Stabilization by Naturally Occurring Osmolytes, *Biochemistry 34*, 12884−12891.
3. Bolen, D. W., and Baskakov, I. V. (2001) The Osmophobic Effect: Natural Selection of a Thermodynamic Force in Protein Folding, *J. Mol. Biol. 310*, 955−963.
4. Lin, T.-Y., and Timasheff, S. N. (1994) Why Do Some Organisms Use a Urea-Methylamine Mixture as Osmolyte? Thermodynamic Compensation of Urea and Trimethylamine *N*-Oxide Interactions with Protein, *Biochemistry 33*, 12695−12701.
5. Yancey, P. H., Clark, M. E., Hand, S. C., Bowlus, R. D., and Somero, G. N. (1982) Living with Water Stress: Evolution of Osmolyte Systems, *Science 217*, 1214−1222.
6. Barone, G., Del Vecchio, P., Esposito, D., Fessas, D., and Graziano, G. (1996) Effect of Osmoregulatory Solutes on the Thermal Stability of Calf-Thymus DNA, *J. Chem. Soc. Faraday Trans. 92*, 1361−1367.
7. Rees, W. A., Yager, T. D., Korte, J., and von Hippel, P. H. (1993) Betaine Can Eliminate the Base Pair Composition Dependence of DNA Melting, *Biochemistry 32*, 137−144.
8. Aslanyan, V. M., Babayan, Y. S., and Arutyunyan, S. G. (1984) Conformation and Thermal Stability of DNA in Aqueous Urea Solutions, *Biophysics 29*, 410−414.
9. Babayan, Y. S. (1988) Conformation and Thermostability of Double-Helical Nucleic Acids in Aqueous Solutions of Urea, *Mol. Biol. (Moscow) 22*, 1204−1210.
10. Klump, H., and Burkart, W. (1977) Calorimetric Measurements of the Transition Enthalpy of DNA in Aqueous Urea Solutions, *Biochim. Biophys. Acta 475*, 601−604.
11. Nordstrom, L. J., Clark, C. A., Andersen, B., Champlin, S. M., and Schwinefus, J. J. (2006) Effect of Ethylene Glycol, Urea, and *N*-Methylated Glycines on DNA Thermal Stability: The Role of DNA Base Pair Composition and Hydration, *Biochemistry 45*, 9604−9614.

12. Gluick, T. C., and Yadav, S. (2003) Trimethylamine *N*-Oxide Stabilizes RNA Tertiary Structure and Attenuates the Denaturing Effects of Urea, *J. Am. Chem. Soc. 125*, 4418−4419.
13. Gluick, T. C., Wills, N. M., Gesteland, R. F., and Draper, D. E. (1997) Folding of an mRNA Pseudoknot Required for Stop Codon Readthrough: Effects of Mono- and Divalent Ions on Stability, *Biochemistry 36*, 16173−16186.
14. Hickey, D. R., and Turner, D. H. (1985) Solvent Effects on the Stability of A_7U_7p, *Biochemistry 24*, 2086−2094.
15. Shelton, V. M., Sosnick, T. R., and Pan, T. (1999) Applicability of Urea in the Thermodynamic Analysis of Secondary and Tertiary RNA Folding, *Biochemistry 38*, 16831−16839.
16. Theimer, C. A., and Giedroc, D. P. (1999) Equilibrium Unfolding Pathway of an H-type RNA Pseudoknot which Promotes Programmed −1 Ribosomal Frameshifting, *J. Mol. Biol. 289*, 1283−1299.
17. Theimer, C. A., Blois, C. A., and Feigon, J. (2005) Structure of the Human Telomerase RNA Pseudoknot Reveals Conserved Tertiary Interactions Essential for Function, *Mol. Cell 17*, 671−682.
18. Theimer, C. A., Finger, L. D., Trantirek, L., and Feigon, J. (2003) Mutations Linked to Dyskeratosis Congenita Cause Changes in the Structural Equilibrium in Telomerase RNA, *Proc. Natl. Acad. Sci. U.S.A. 100*, 449−454.
19. Milligan, J., and Uhlenbeck, O. (1989) Synthesis of Small RNAs Using T7 RNA Polymerase, *Methods Enzymol. 180*, 51−62.
20. Laing, L. G., and Draper, D. E. (1994) Thermodynamics of RNA Folding in a Conserved Ribosomal RNA Domain, *J. Mol. Biol. 237*, 560−576.
21. Theimer, C. A., Wang, Y., Hoffman, D. W., Krisch, H. M., and Giedroc, D. P. (1998) Non-nearest Neighbor Effects on the Thermodynamics of Unfolding of a Model mRNA Pseudoknot, *J. Mol. Biol. 279*, 545−564.
22. Hong, J., Capp, M. W., Anderson, C. F., Saecker, R. M., Felitsky, D. J., Anderson, M. W., and Record, M. T., Jr. (2004) Preferential Interactions of Glycine Betaine and of Urea with DNA: Implications for DNA Hydration and for Effects of These Solutes on DNA Stability, *Biochemistry 43*, 14744−14758.
23. Courtenay, E. S., Capp, M. W., Anderson, C. F., and Record, M. T., Jr. (2000) Vapor Pressure Osmometry Studies of Osmolyte-Protein Interactions: Implications for the Action of Osmoprotectants in Vivo and for the Interpretation of "Osmotic Stress" Experiments in Vitro, *Biochemistry 39*, 4455−4471.
24. Courtenay, E. S., Capp, M. W., Saecker, R. M., and Record, M. T., Jr. (2000) Thermodynamic Analysis of Interactions Between Denaturants and Protein Surface Exposed on Unfolding: Interpretation of Urea and Guanidinium Chloride m-Values and Their Correlation With Changes in Accessible Surface Area (ASA) Using Preferential Interaction Coefficients and the Local-Bulk Domain Model, *Proteins: Struct., Funct., Genet. 4*, 72−85.
25. Felitsky, D. J., and Record, M. T., Jr. (2004) Application of the Local-Bulk Partitioning and Competitive Binding Models to Interpret Preferential Interactions of Glycine Betaine and Urea with Protein Surface, *Biochemistry 43*, 9276−9288.
26. Record, M. T., Jr., Zhang, W., and Anderson, C. F. (1998) Analysis of Effects of Salts and Uncharged Solutes on Protein and Nucleic Acid Equilibria and Processes: A Practical Guide to Recognizing and Interpreting Polyelectrolyte Effects, Hofmeister Effects, and Osmotic Effects of Salts, *Adv. Protein Chem. 51*, 281−353.
27. Wyman, J. (1965) The Binding Potential, A Neglected Linkage Concept, *J. Mol. Biol. 11*, 631−644.
28. Wyman, J. J. (1964) Linked Functions and Reciprocal Effects in Hemoglobin: A Second Look, *Adv. Protein Chem. 19*, 223−286.
29. Moore, W. J. (1972) Solutions, in *Physical Chemistry*, Prentice Hall, Inc., Upper Saddle River, NJ.
30. Spink, C. H., and Chaires, J. B. (1999) Effects of Hydration, Ion Release, and Excluded Volume on the Melting of Triplex and Duplex DNA, *Biochemistry 38*, 496−508.
31. Moore, W. J. (1972) Chemical Affinity, in *Physical Chemistry*, Prentice Hall, Inc., Upper Saddle River, NJ.
32. Scatchard, G., Hamer, W. J., and Wood, S. E. (1938) Isotonic Solutions. I. The Chemical Potential of Water in Aqueous Solutions of Sodium Chloride, Potassium Chloride, Sulfuric Acid, Sucrose, Urea and Glycerol at 25°, *J. Am. Chem. Soc. 60*, 3061−3070.
33. Smith, P. K., and Smith, E. R. B. (1940) Thermodynamic Properties of Solutions of Amino Acids and Related Substances. V. The Activities of Some Hydroxy- and N-Methylamino Acids and Proline in Aqueous Solution at Twenty-Five Degrees, *J. Biol. Chem. 132*, 57−64.
34. Tsodikov, O. V., Record, M. T., Jr., and Sergeev, Y. V. (2002) Novel Computer Program for Fast Exact Calculation of Accessible and Molecular Surface Areas and Average Surface Curvature, *J. Comput. Chem. 23*, 600−609.
35. Richards, F. M. (1977) Areas, Volumes, Packing, and Protein Structure, *Annu. Rev. Biophys. Bioeng. 6*, 151−176.
36. Turner, D. H., Sugimoto, N., and Freier, S. M. (1988) RNA Structure Prediction, *Annu. Rev. Biophys. Biophys. Chem. 17*, 167−192.
37. Xia, T., SantaLucia, J. J., Burkard, M. E., Kierzek, R., Schroeder, S. J., Jiao, X., Cox, C., and Turner, D. H. (1998) Thermodynamic Parameters for an Expanded Nearest-Neighbor Model for Formation of RNA Duplexes with Watson-Crick Base Pairs, *Biochemistry 37*, 14719−14735.
38. Felitsky, D. J., and Record, M. T., Jr. (2003) Thermal and Urea-Induced Unfolding of the Marginally Stable Lac Repressor DNA-Binding Domain: A Model System for Analysis of Solute Effects on Protein Processes, *Biochemistry 42*, 2202−2217.
39. Felitsky, D. J., Cannon, J. G., Capp, M. W., Hong, J., Van Wynsberghe, A. W., Anderson, C. F., and Record, M. T., Jr. (2004) The Exclusion of Glycine Betaine from Anionic Biopolymer Surface: Why Glycine Betaine is an Effective Osmoprotectant but Also a Compatible Solute, *Biochemistry 43*, 14732−14743.
40. Arakawa, T., and Timasheff, S. N. (1983) Preferential Interactions of Proteins with Solvent Components in Aqueous Amino Acid Solutions, *Arch. Biochem. Biophys. 224*, 169−177.
41. Zhang, W., Capp, M. W., Bond, J. P., Anderson, C. F., and Record, M. T., Jr. (1996) Thermodynamic Characterization of Interactions of Native Bovine Serum Albumin with Highly Excluded (Glycine Betaine) and Moderately Accumulated (Urea) Solutes by a Novel Application of Vapor Pressure Osmometry, *Biochemistry 35*, 10506−10516.
42. Hong, J., Capp, M. W., Anderson, C. F., and Record, M. T., Jr. (2003) Preferential Interactions in Aqueous Solutions of Urea and KCl, *Biophys. Chem. 105*, 517−532.
43. Chalikian, T. V., Völker, J., Srinivasan, A. R., Olson, W. K., and Breslauer, K. J. (1999) The Hydration of Nucleic Acid Duplexes as Assessed by a Combination of Volumetric and Structural Techniques, *Biopolymers 50*, 459−471.
44. Feig, M., and Pettitt, B. M. (1998) A Molecular Simulation Picture of DNA Hydration Around A- and B-DNA, *Biopolymers 48*, 199−209.
45. Mohan, V., Smith, P. E., and Pettitt, B. M. (1993) Evidence for a New Spine of Hydration: Solvation of DNA Triple Helices, *J. Am. Chem. Soc. 115*, 9297−9298.
46. Mrevlishvili, G. M., Carvalho, A. P. S. M. C., and da Silva, M. A. V. R. (2002) Low-Temperature DSC Study of the Hydration of ss-DNA and ds-DNA and the Role of Hydrogen-Bonded Network to the Duplex Transition Thermodynamics, *Thermochim. Acta 394*, 73−82.
47. Radhakrishnan, I., and Patel, D. J. (1994) DNA Triplexes: Solution Structures, Hydration Sites, Energetics, Interactions, and Function, *Biochemistry 33*, 11405−11416.
48. Sundaralingam, M., and Pan, B. (2002) Hydrogen and Hydration of DNA and RNA Oligonucleotides, *Biophys. Chem. 95*, 273−282.

BI602637V